Available online at www.sciencedirect.com
ScienceDirect
Carbohydrate Research 342 (2007) 1480–1489
Carbohydrate RESEARCH

Experimental charge density of sucrose at 20 K: bond topological, atomic, and intermolecular quantitative properties

Da'san M. M. Jaradat,[a,b] Stefan Mebs,[a] Lilianna Chęcińska[a,c] and Peter Luger[a,*]

[a]*Institute for Chemistry and Biochemistry/Crystallography, Free University Berlin, Fabeckstraße 36a, 14195 Berlin, Germany*
[b]*Industrial Chemistry Center, Royal Scientific Society, PO Box 1438, Al-Jubaiha 11941, Amman, Jordan*
[c]*Department of Crystallography and Crystal Chemistry, University of Łódź, Pomorska 149/153, 90236 Łódź, Poland*

Received 26 January 2007; received in revised form 29 March 2007; accepted 2 April 2007
Available online 21 April 2007

Dedicated to Professor Dr. Hans Paulsen on the occasion of his 85th birthday

Abstract—The charge density of sucrose was determined from a high-resolution X-ray data set measured at 20 K. The density distribution so obtained was analyzed quantitatively by application of Bader's atoms in molecules (AIM) formalism, and a comparison was made with corresponding results from a B3LYP (6-311++G(3df,3pd)) calculation at the experimental geometry. Bond topological and atomic properties (volumes and charges) were derived and compared. The influence of hydrogen bonding on the experimental charge density was also studied qualitatively and quantitatively by means of topological properties. In terms of the hydrogen-bond energies, a grouping into strong, medium and very weak hydrogen bonds was made, the latter of which were involved in a bifurcated bond.

Keywords: Sucrose; Charge density; Topological analysis

1. Introduction

Sugar and salt, more precisely, sucrose and sodium chloride, are the only substances people consume daily in the crystalline state. It is therefore understandable that these two compounds played a remarkable role in the history of crystallographic research, however, in different ways. While sodium chloride, the first crystal structure ever reported, was published in 1913,[1] only one year after the discovery of X-ray diffraction, sucrose was a practically unsolvable problem for almost half a century. In the scope of X-ray analysis, sucrose had to be considered as a 'large' molecule of complicated geometry, so that it took until 1952, when the first X-ray analysis on sucrose was published. At that time the structure was based on two-dimensional projections, with a hint by the authors that the study took ~8 years to be finished.[2] Three-dimensional neutron and X-ray structures were not published before the sixties and seventies at currently accepted accuracy.[3–5]

For charge-density work, sucrose and most other carbohydrates were also considered as 'large' or even too large molecules (although some first X–N difference density maps were shown in Ref. 5) so that experimental charge-density studies on carbohydrates or related model compounds were carried out only in exceptional cases[6–8] due to the time-consuming nature of the high-resolution X-ray diffraction experiment. Thanks to the recent technical and methodological advances, charge-density analyses can now be performed in a reasonable time and provide quantitative information on atomic and intra- and intermolecular bonding properties, so that, for example, hydrogen bonds, which play a major role in most carbohydrate structures, can be characterized quantitatively from the topology of their charge density. This encouraged us to enter into an experimental and theoretical investigation of the charge-density

* Corresponding author. Tel.: +49 30 838 53411; fax: +49 30 838 53464; e-mail: luger@chemie.fu-berlin.de

0008-6215/$ - see front matter © 2007 Elsevier Ltd. All rights reserved.
doi:10.1016/j.carres.2007.04.004

distribution of sucrose, which has never been reported in detail according to our knowledge, of which the results are reported here.

The charge density $\rho(\vec{r})$ of a chemical structure can be obtained either theoretically from high-level ab initio calculations or experimentally by a multipole refinement of high-resolution X-ray diffraction data at low temperature.[9] In Bader's theory of atoms in molecules (AIM),[10] the charge density plays a central role. In general, the topological analysis of $\rho(\vec{r})$ allows a quantitative description of bonds, nonbonding interactions, electronic structure, and reactivity. Moreover, a well-defined procedure of partitioning a molecule into atomic regions is provided, making use of the zero-flux surfaces (ZFS) in the electron-density gradient vector field $\nabla\rho(\vec{r})$. Surfaces of this type establish atomic basins around nuclear attractors of the corresponding trajectories of $\nabla\rho(\vec{r})$. As a result, each basin uniquely defines an atomic volume. Once the shape and the volume of an atom are known, a number of atomic or functional group properties can be evaluated; for instance, atomic charges can be obtained by integration over the charge density in the given atomic volume.

For an experimental charge-density determination, more than 86,370 reflections of a sucrose crystal were collected at 20 K using Mo Kα radiation. This data set was the subject of multipole refinement, and the resulting model densities were analyzed quantitatively in terms of Bader's AIM theory. The theoretical density distribution was derived from ab initio methods. The program package GAUSSIAN 98[11] was used for a single-point density functional calculation based on the experimental geometry with the basis set B3LYP (6-311++G(3df,3pd)). The wave function obtained was evaluated with the program MORPHY 98.[12]

2. Experimental and refinement calculations

2.1. Data collection and structure solution

A colorless single crystal of commercially available sucrose with dimensions of $0.40 \times 0.35 \times 0.30\ \text{mm}^3$ was selected under a light microscope. A high-resolution X-ray data set at 20 K was collected on a large four-circle Eulerian cradle diffractometer (Huber, type 512) equipped with a double-stage, closed-cycle He refrigerator (Displex, Air Products, USA) with an APEX CCD area detector, using Mo Kα radiation. A 0.1 mm Kapton film cylinder was used as vacuum chamber as described in Ref. 13. The data collection was monitored with SMART, and the frames were integrated using SAINT,[14] while the data reduction was performed using SadXp (SADABS and XPREP).[15] Although known from the literature, the structure was resolved from the 20 K data using SHELXS 97[16] and spherically refined with the program SHELXL 97.[17] Further details on the crystal data and the experimental conditions are given in Table 1.

Table 1. Crystal data and structure refinement for sucrose

Empirical formula	$C_{12}H_{22}O_{11}$
Formula weight	342.30
Temperature	20(2) K
Wavelength	0.71073 Å
Crystal system, space group	Monoclinic, $P2_1$
Unit cell dimensions	$a = 7.736(3)$ Å, $\alpha = 90°$ $b = 8.702(4)$ Å, $\beta = 102.97(2)°$ $c = 10.846(5)$ Å, $\gamma = 90°$
Cell volume/Z	711.5(6) Å^3/2
Density (calculated)	1.598 Mg/m^3
Absorption coefficient	0.143 mm^{-1}
Crystal size	$0.40 \times 0.35 \times 0.30$ mm^3
$(\sin\theta/\lambda)_{max}$	1.15 Å^{-1}
Reflections collected	86,373
Independent reflections (all data)	8732 [$R_{(int)} = 0.0137$]
Redundancy	9.9
Independent reflections [$I > 2\sigma(I)$]	8481
Completeness to $(\sin\theta/\lambda)_{max}$	93.2%
Spherical atom refinement	
Data/restraints/parameters	8732/1/296
Goodness-of-fit on F^2	1.069
Final R indices [$I > 2\sigma(I)$]	$R_1 = 0.0267$, $wR_2 = 0.0694$
R indices (all data)	$R_1 = 0.0281$, $wR_2 = 0.0702$
Absolute structure parameter	0.1(2)
Multipole atom refinement	
Number of data	8732
Rejected reflections	406
Included in the refinement	8326
R_1	0.0182
$R_{1(all)}$	0.0201
Gof	1.7062
wR_F	0.0149
N_{ref}/N_v	12.2082

$R_1 = \sum||F_o| - |F_c||/\sum|F_o|$; $wR_2 = \left[\sum w(|F_o|^2 - |F_c|^2)^2/\sum w|F_o|^4\right]^{1/2}$.

$wR_F = \left[\sum w(|F_o| - |F_c|)^2/\sum w|F_o|^2\right]^{1/2}$.

$\text{Gof} = \left[\sum w(|F_o|^2 - |F_c|^2)^2/(N_{ref} - N_v)\right]^{1/2}$.

2.2. Multipole refinement

The independent data set was refined using the Hansen and Coppens multipole formalism[18] as implemented in the program package XD,[19] using a weighting scheme $w = 1/\sigma^2(F_o)$. The starting atomic parameters were taken from the spherical atom refinement. In the multipole formalism the core and the spherical valence densities of the heavy atoms were composed of Hartree–Fock wave functions expanded over Slater-type basis functions. For the deformation terms single-zeta orbitals with energy-optimized Slater exponents were taken and kept fixed.[20] Additional to the positional and thermal parameters (anisotropic for C and N, isotropic for H), populations up to hexadecapolar level for carbon and oxygen atoms and bond-directed dipoles for hydrogen atoms ($P_{valence}$ and P_{lm}, Eq. 1) were refined together with expansion/contraction parameters κ in the least-squares procedure:

$$\rho_{\text{atom}}(\vec{r}) = \rho_{\text{core}}(\vec{r}) + P_{\text{valence}}\kappa^3\rho_{\text{valence}}(\kappa\vec{r}) + \rho_{\text{deformation}}$$
$$\text{with } \rho_{\text{deformation}} = \sum_{l=0}^{4}\kappa'^3 R_l(\kappa'\vec{r})\sum_{m=0}^{l}P_{lm\pm}Y_{lm\pm}(\theta,\varphi) \quad (1)$$

In order to reduce the number of variables, it is a common practice to constrain multipole parameters to be equal for chemically equivalent atoms; therefore, C(2), C(3), C(3′), and C(4′) were constrained to C(4), and similarly H(2), H(3), H(3′), and H(4′) were constrained to H(4). Furthermore, H(62), H(11′), H(12′), H(61′), and H(62′) were constrained to H(61), while the populations of the other hydrogen atoms were refined without any constraints. No symmetry restriction was imposed on any atom of sucrose. Bonds to H atoms were set to the neutron distances from Ref. 4. Four κ parameters were assigned (and refined, except the one for H) as follows: All oxygens of the hydroxyl groups were assigned a κ_1, and for the other oxygen atoms a κ_2 was selected. Since all carbon atoms have sp^3 hybridization, they were assigned a κ_3 and all hydrogen atoms a κ_4.

3. Results and discussion

3.1. Charge density and topological analysis

The numbering scheme and displacement ellipsoids of the asymmetric unit of sucrose, which consists of one molecule, are illustrated in Figure 1 by an ORTEP representation.[21] The molecular geometry is well known and needs no further discussion. Our structure at 20 K shows bond lengths generally slightly longer by 0.5–0.7% compared to the room temperature X-ray/neutron[4,5] results due to reduced thermal motion. Otherwise, there is no difference from the previous very accurate sucrose crystal structure analyses.

In Figure 2 (top) static deformation densities are shown in the endocyclic C–O–C planes. For all bonds one maximum between the corresponding atoms signifies the covalent character of all bonds. An additional local maximum of the valence shell charge concentration (VSCC) is visible for the oxygen atoms, which corresponds to the lone-pair regions. Qualitatively, more density is seen on the C–O bonds C(1)–O(5) and C(2′)–O(2′) compared to the two other endocyclic C–O bonds as will be detailed quantitatively below.

The residual density maps in Figure 2 (bottom) are practically featureless, indicating the proper deconvolution of the experimental density by the multipole model.

For a quantitative description of the electronic structure, a full topological analysis was carried out with the XDPROP program of the XD program package.[19] In the gradient vector field $\nabla\rho(\vec{r})$ of the electron density, critical points (CPs) defined after Bader[10] by the property that $\nabla\rho(\vec{r})$ vanishes at a CP play a special role. Two types of critical points were found: bond critical points (BCPs) for all covalent and hydrogen bonds and ring critical points (RCPs) for the furanosyl and pyranosyl rings. In addition, the intramolecular hydrogen bondings O(1′)–H(1O′)···O(2) and O(6′)–H(6O′)···O(5) establish eight- and nine-membered ring structures, respectively, and in both of them ring critical points of low electron density (0.063 and 0.035 e Å^{-3}, respectively) were identified.

Table 2 gives a summary of quantitative, experimental and theoretical topological properties at the bond critical points for the O–C and C–C bonds of sucrose. The topological properties were also averaged for the eight exocyclic O–C and the 10 C–C single bonds (Table 2) in order to make a general comparison and to see the

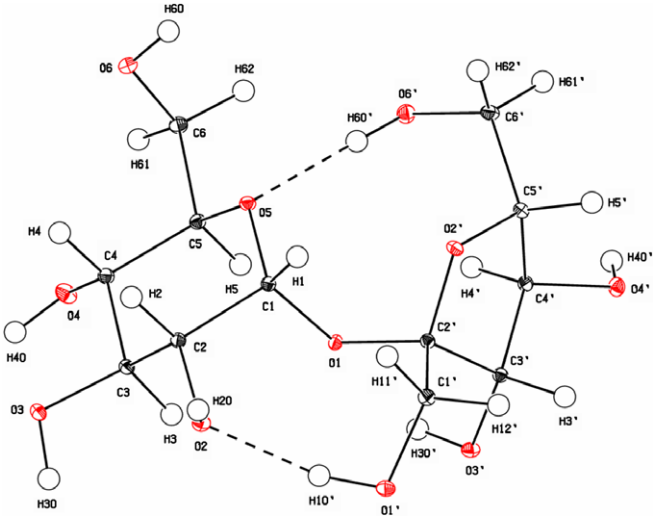

Figure 1. Molecular structure of sucrose showing 50% thermal ellipsoids at 20 K. ORTEP[21] representation: hydrogen atoms are drawn as small spheres of arbitrary radii.

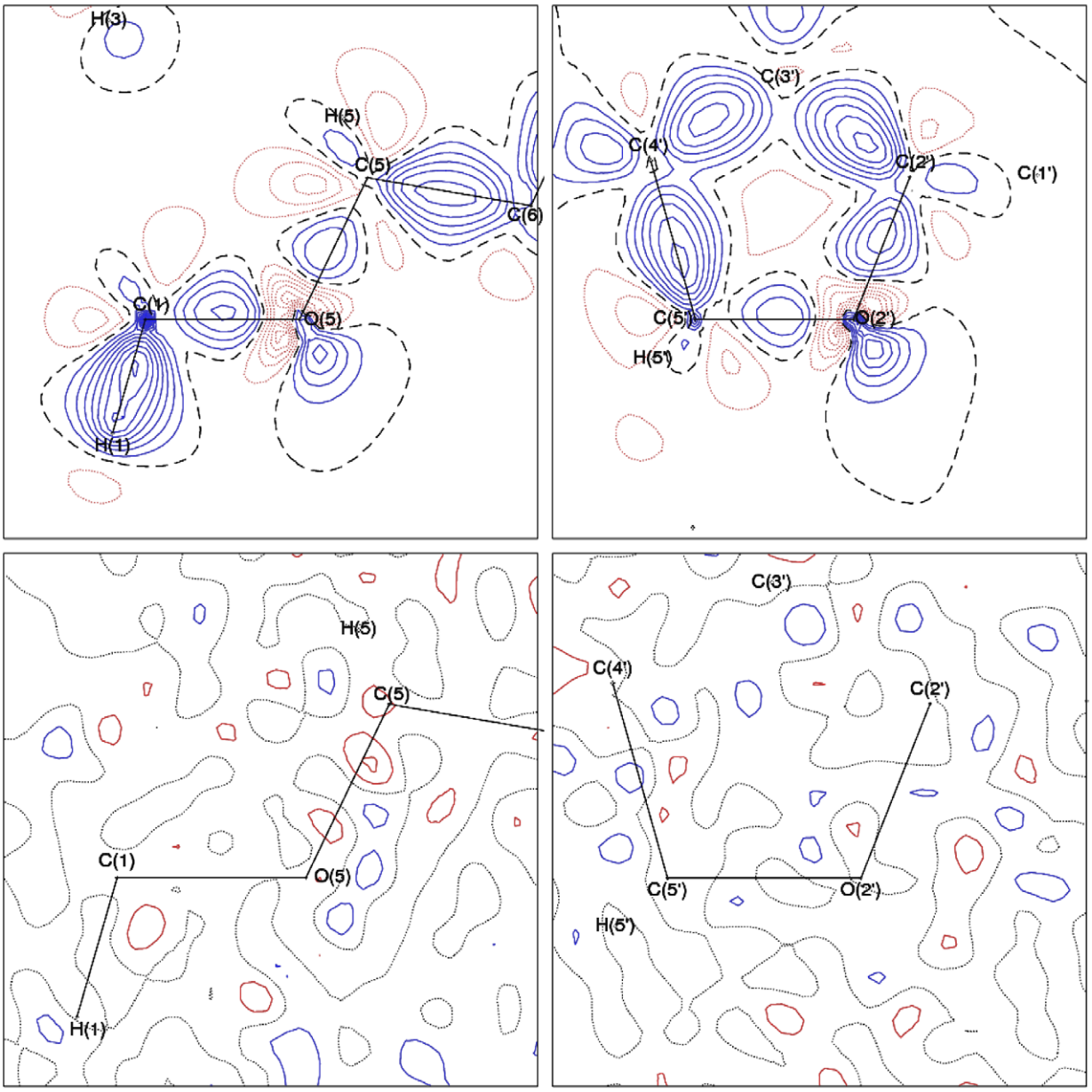

Figure 2. Static deformation density maps (top) and residual density maps (bottom) in the endocyclic C–O–C planes. Positive, negative, and zero contours are represented by blue solid, red dotted, and black dashed lines, respectively. Contour intervals at 0.1 e $Å^{-3}$.

trend of each bond class in terms of theoretical and experimental parameters. For the nonpolar C–C single bonds, there is a very good agreement between the results of the experimental and the theoretical topological analysis. For these bonds the electron-density values at the BCP, $\rho(\vec{r}_b)$, differ by 0.04 e $Å^{-3}$ (average) between experiment and theory, while the corresponding difference for the Laplacians is 0.2 e $Å^{-5}$. For the endocyclic O–C bonds to the anomeric carbon atoms (O(5)–C(1) in the pyranosyl ring, O(2′)–C(2′) in the furanosyl ring), it can be seen that, as an implication of the anomeric effect, these bonds are the strongest with a 10–20% higher value of the electron density at the BCP than on the bonds O(5)–C(5) and O(2′)–C(5′). For the eight exocyclic C–O(H) bonds, we find an experimental average $\rho(\vec{r}_b)$ value (1.90(4) e $Å^{-3}$), which is higher than that of theory (1.74(3) e $Å^{-3}$) by 8.5%. These differences between experiment and theory, particularly, for the Laplacians at the BCPs of polar bonds, are well known and are attributed to the nature of the radial functions in the experimental multipole model.[22] The large $\rho(\vec{r}_b)$ values and the negative signs of $\nabla^2\rho(\vec{r}_b)$ for all bonds in Table 2 are an evidence of the presence of shared-shell interactions that correspond to the covalent bonds occurring in the sucrose molecule.

Further comparison is made in Table 3 between experimental and theoretical models in terms of ring critical points $\vec{r}_r$. It can be seen from the values in Table

Table 2. Experimental and theoretical bond topological properties $\rho(\vec{r}_b)$, $\nabla^2\rho(\vec{r}_b)$ (in e Å^{-3} and e Å^{-5}, respectively) and the ellipticity ε, bond distances d in Å

Bond	$\rho(\vec{r}_b)$[a]	$\nabla^2\rho(\vec{r}_b)$[a]	ε[a]	d	$\rho(\vec{r}_b)$[b]	$\nabla^2\rho(\vec{r}_b)$[b]	ε[b]
O(1)–C(1)	1.99(3)	−14.6(1)	0.05	1.4304(4)	1.76	−15.2	0.09
O(1)–C(2′)	1.85(3)	−15.6(2)	0.05	1.4388(4)	1.71	−14.0	0.15
O(2)–C(2)	1.90(2)	−13.2(1)	0.06	1.4329(6)	1.69	−12.1	0.02
O(3)–C(3)	1.92(2)	−12.3(1)	0.12	1.4360(5)	1.71	−13.3	0.02
O(4)–C(4)	1.90(2)	−13.3(1)	0.08	1.4221(4)	1.75	−13.4	0.02
O(5)–C(1)	1.96(4)	−21.2(2)	0.11	1.4192(5)	1.80	−15.4	0.10
O(5)–C(5)	1.75(4)	−15.8(2)	0.18	1.4477(4)	1.63	−11.3	0.02
O(6)–C(6)	1.91(3)	−17.4(1)	0.06	1.4282(4)	1.72	−12.7	0.00
O(1′)–C(1′)	1.84(2)	−14.2(1)	0.05	1.4344(5)	1.75	−15.1	0.02
O(2′)–C(2′)	2.05(3)	−21.0(2)	0.03	1.4146(5)	1.82	−15.2	0.10
O(2′)–C(5′)	1.71(4)	−13.3(2)	0.08	1.4543(5)	1.63	−11.8	0.02
O(3′)–C(3′)	1.95(2)	−15.7(1)	0.07	1.4131(4)	1.81	−14.7	0.01
O(4′)–C(4′)	1.95(2)	−13.8(1)	0.09	1.4272(4)	1.74	−13.6	0.02
O(6′)–C(6′)	1.84(2)	−13.6(1)	0.11	1.4349(4)	1.72	−13.7	0.01
C(1)–C(2)	1.78(2)	−15.1(1)	0.07	1.5432(5)	1.71	−15.0	0.08
C(2)–C(3)	1.74(2)	−14.8(1)	0.02	1.5328(4)	1.72	−15.0	0.04
C(3)–C(4)	1.75(1)	−14.8(1)	0.03	1.5330(5)	1.72	−15.0	0.03
C(4)–C(5)	1.72(2)	−15.1(1)	0.20	1.5351(5)	1.71	−14.9	0.09
C(5)–C(6)	1.74(3)	−13.8(1)	0.04	1.5301(5)	1.72	−15.2	0.06
C(1′)–C(2′)	1.82(3)	−16.2(1)	0.18	1.5310(5)	1.75	−15.8	0.08
C(2′)–C(3′)	1.77(2)	−14.6(1)	0.11	1.5492(4)	1.69	−14.6	0.08
C(3′)–C(4′)	1.75(2)	−14.6(1)	0.02	1.5320(5)	1.72	−14.9	0.03
C(4′)–C(5′)	1.80(2)	−15.4(1)	0.09	1.5372(4)	1.70	−14.6	0.08
C(5′)–C(6′)	1.76(3)	−14.2(1)	0.10	1.5217(5)	1.75	−15.6	0.03
O–Cexo[c]	1.90(4)	−14.2(15)	0.08(2)		1.74(3)	−13.6(9)	0.02(1)
C–C[c]	1.76(3)	−14.9(6)	0.09(6)		1.72(2)	−15.1(4)	0.06(4)

[a] Experimentally obtained from XDPROP program of the XD package.
[b] Theoretically derived from B3LYP (6-311++G(3df,3pd)).
[c] Averaged over the eight exocyclic C–O(H) bonds and the 10 C–C single bonds.

Table 3. Experimental and theoretical ring critical point (RCP) properties $\rho(\vec{r}_r)$, $\nabla^2\rho(\vec{r}_r)$ in e Å^{-3} and e Å^{-5}, respectively

Ring	$\rho(\vec{r}_r)$[a]	$\nabla^2\rho(\vec{r}_r)$[a]	$\rho(\vec{r}_r)$[b]	$\nabla^2\rho(\vec{r}_r)$[b]
1	0.26	6.0	0.29	6.0
2	0.14	2.6	0.14	2.8
3	0.06	1.1	0.07	1.0
4	0.03	0.6	0.04	0.6

Ring 1: O(2′)–C(2′)–C(3′)–C(4′)–C(5′), ring 2: O(5)–C(1)–C(2)–C(3)–C(4)–C(5), ring 3: C(1)–O(1)–C(2′)–C(1′)–O(1′)–H(1O′)–O(2)–C(2), ring 4: C(2′)–O(1)–C(1)–O(5)–H(6O′)–O(6′)–C(6′)–C(5′)–O(2′).
[a] Experimentally obtained from XDPROP program of the XD package.
[b] Theoretically derived from B3LYP (6-311++G(3df,3pd)).

3 that both models, the experimental and the theoretical, are in an excellent agreement with each other and that $\rho(\vec{r}_r)$ and $\nabla^2\rho(\vec{r}_r)$ values decrease by moving from ring 1 to ring 4, which is attributed to the fact that small-sized rings have greater values of topological properties at an RCP than large-sized rings due to the closeness of atoms to each other.

As already mentioned, Bader's AIM theory allows a subdivision of molecules into submolecular regions, fragments or single atoms making use of the zero-flux surfaces (ZFS) of the electron-density gradient vector field. The integration procedure available through the TOPXD[23] program as part of XD[19] was applied to evaluate atomic volumes and charges. The results are summarized for all atoms of the title compound in Table 4. The total atomic volumes V_{tot} are defined by the interatomic boundaries in the crystal. It is a common practice to consider also the V_{001} volumes, defined by a cutoff at $\rho = 0.001$ au, which are useful for comparison with corresponding properties obtained from theoretical calculations for isolated molecules. Since the charge density in the outer regions of an atomic basin does not contribute substantially to its charge, the net atomic charges q_{tot} and q_{001} are in most cases practically equal, so that only one charge column q is given in Table 4.

Bader atomic volumes and charges are additive; therefore, the sum of atomic volumes in one unit cell should be equal to the experimental cell volume. Similarly, the sum of all atomic charges should add up to zero. Summation for sucrose shows that the integration routine has worked properly as the experimental unit cell volume $V_{exp} = 711.5(6)$ Å^3 (Table 1) and $\sum V_{tot} = 708.1$ Å^3 (multiplied by $Z = 2$) differ by less than 1%, and $\sum q$ differs by only 0.04 e from electroneutrality.

For the oxygen atoms it is easy to see that O(5) and O(2′) and the glycosidic oxygen O(1), having in common to be the center of a C–O–C-sequence, have a small volume around 12 Å^3 while the hydroxyl oxygens (C–O–H-sequence) have a larger volume, averaging to 16.9(8) Å^3

Table 4. Summary of experimental atomic volumes V_{tot} and V_{001} in Å^3, and the net atomic charges q in e

Atom	V_{tot}	V_{001}	q
O(1)	12.30	12.23	−1.04
O(2)	16.86	15.54	−1.13
O(3)	18.23	16.17	−1.03
O(4)	16.98	15.65	−1.07
O(5)	11.85	11.69	−0.98
O(6)	15.73	15.49	−1.16
O(1′)	16.26	15.27	−1.09
O(2′)	12.74	12.23	−0.99
O(3′)	16.21	15.41	−1.14
O(4′)	17.91	16.09	−1.11
O(6′)	16.93	15.53	−1.10
C(1)	5.76	5.74	0.62
C(2)	5.75	5.75	0.53
C(3)	5.62	5.60	0.53
C(4)	5.73	5.73	0.51
C(5)	6.82	6.76	0.36
C(6)	8.17	7.91	0.35
C(1′)	7.56	7.52	0.34
C(2′)	4.86	4.86	0.72
C(3′)	5.83	5.78	0.53
C(4′)	5.89	5.89	0.53
C(5′)	6.70	6.69	0.33
C(6′)	8.25	7.84	0.35
H(1)	4.55	4.47	0.15
H(2)	7.19	5.82	−0.02
H(3)	6.22	5.99	−0.04
H(4)	5.99	5.29	−0.02
H(5)	6.92	5.69	0.22
H(61)	7.92	5.98	0.16
H(62)	7.05	5.95	0.15
H(11′)	5.29	5.29	0.16
H(12′)	6.40	6.14	0.14
H(3′)	6.23	5.68	−0.02
H(4′)	6.18	5.45	−0.03
H(5′)	6.40	5.35	0.17
H(61′)	5.41	5.37	0.15
H(62′)	7.66	5.67	0.15
H(2O)	1.67	1.66	0.67
H(3O)	2.32	2.24	0.56
H(4O)	2.52	2.45	0.60
H(6O)	1.59	1.59	0.63
H(1O′)	2.28	2.19	0.51
H(3O′)	1.40	1.40	0.69
H(4O′)	1.60	1.58	0.64
H(6O′)	2.29	2.17	0.55
Sum	354.03	330.80	0.04

for V_{tot} and 15.6(3) Å^3 for V_{001}. A difference in the charges for these two types of oxygens is not seen. They all carry a negative charge around −1 e (average −1.08(6) e).

All carbon atoms are sp^3 hybridized; nevertheless, the methoxy carbons C(6), C(1′), and C(6′) having two hydrogens as nearest neighbors have larger volumes, being around 8 Å^3, while the ring carbons with one hydrogen less as nearest neighbors have volumes, which vary between 5 and 6 Å^3, except for C(5) and C(5′), which have a volume close to 6.7 Å^3. The reasons for these observed changes in volumes are not apparent. For the carbon atoms, the different volumes also lead to different charges, in that the positive charges behave inverse to the volume size.

All hydrogens bonded to carbon atoms have volumes roughly between 4.5 and 8 Å^3 and charges not far from zero. The OH hydrogens, all of which contribute to hydrogen bonds, have significantly smaller volumes between 1.4 and 2.5 Å^3 and positive charges around 0.5–0.7 e. These properties of decreased volumes and increased positive charges were already part of various criteria expressed by Koch and Popelier[24] for hydrogen-bonded hydrogen atoms. However, these authors hestitated in giving the volume decrease the 'status of a necessary condition'. In most cases where OH hydrogen atomic properties were determined so far, the corresponding hydrogen atoms were involved in hydrogen bonds; however, we have observed two examples (codeine[25] and the tripeptide L-Ala-L-Pro-L-Ala[26]) where OH hydrogens did not contribute to hydrogen bonds but had small volumes as found in this study, so that this is a question to be further explored.

3.2. Hydrogen bonding and electrostatic potential

Topological analysis of charge-density distributions provides additional topological parameters of noncovalent intra- and intermolecular interactions and can therefore lead to a deeper insight into the strength of these interactions.[24,27] In the asymmetric unit of sucrose, nine hydrogen bonds (HBs) according to the potential O–H donors were found (Table 5), two of which are intramolecular and the rest are intermolecular hydrogen bonds.

For the intramolecular HBs the influences of these interactions are illustrated qualitatively in the static maps shown in Figure 3 (top). A precise look at these maps reveals that the electron-density cloud referring to the lone-pair electrons of the accepting O(2) is more shifted toward H(1O′) than that of O(5) shifted toward H(6O′). This observation might be attributed to the stronger HB of O(1′)–H(1O′)···O(2), which contributes in making O(2) more negative and H(1O′) more positive. Experimental residual maps identified in the same planes of the intramolecular HBs (Fig. 3, bottom) do not show any significant residues of the electron density. No contours greater than 0.1 e Å^{-3} could be found after the multipole refinement, indicating again a proper representation of the experimental density by the multipole model.

A closer look at Table 5 shows that the donating atom O(4) is involved in bifurcated hydrogen bonds, which results in two very weak intermolecular hydrogen bonds; O(4)–H(4O)···O(2′) and O(4)–H(4O)···O(6). Originally, in Ref. 4 the hydroxyl group O(4)–H was doubted to be the donor of a hydrogen bond; however, the existence of critical points on both bond paths

Table 5. Summary of hydrogen bonds including geometric and bond topological properties ($\rho(\vec{r}_b)$,$\nabla^2\rho(\vec{r}_b)$, and λ_3 in e Å^{-3} and e Å^{-5}, respectively, distances and angles in Å and deg, E_{HB} in kJ mol^{-1})

D–H···A	Sym./transl.	$\rho(\vec{r}_b)$	$\nabla^2\rho(\vec{r}_b)$	D–H	H···A	D···A	D–H···A	EHB	λ_3
O(1′)–H(1O′)···O(2)	x, y, z	0.17(3)	3.9(1)	0.9732	1.8366	2.7762(5)	161.37	34.0	5.64
O(2)–H(2O)···O(6′)	$-1+x, y, z$	0.11(2)	3.4(1)	0.9718	1.8734	2.8346(6)	169.53	29.8	4.46
O(3)–H(3O)···O(3′)	$-x, -\frac{1}{2}+y, 1-z$	0.15(2)	3.4(1)	0.9583	1.8808	2.8350(5)	173.54	29.0	4.99
O(3′)–H(3O′)···O(4′)	$1-x, -\frac{1}{2}+y, 1-z$	0.11(2)	3.1(1)	0.9675	1.8831	2.8308(5)	165.70	28.8	4.14
O(4)–H(4O)···O(2′)	$x, -1+y, z$	0.09(1)	1.4(1)	0.9113	2.3227	2.8148(6)	113.65	5.9	2.01
O(4)–H(4O)···O(6)	$-x, -\frac{1}{2}+y, -z$	0.04(1)	0.7(1)	0.9113	2.4989	3.3581(6)	157.33	3.1	0.94
O(4′)–H(4O′)···O(1′)	$-x, -\frac{1}{2}+y, -z$	0.17(3)	4.8(1)	0.9758	1.7438	2.7063(6)	168.20	47.5	6.61
O(6)–H(6O)···O(3)	$-x, \frac{1}{2}+y, -z$	0.09(3)	3.6(1)	0.9550	1.8727	2.8116(6)	167.04	29.9	4.53
O(6′)–H(6O′)···O(5)	x, y, z	0.16(2)	3.3(1)	0.9706	1.8856	2.8327(6)	164.49	28.5	4.94

D denotes the donating and A denotes the accepting atoms. Further quantitative energetic and geometrical properties described in the literature for the analysis of HBs based on topological data[24,27,36] are summarized in Supplementary data.

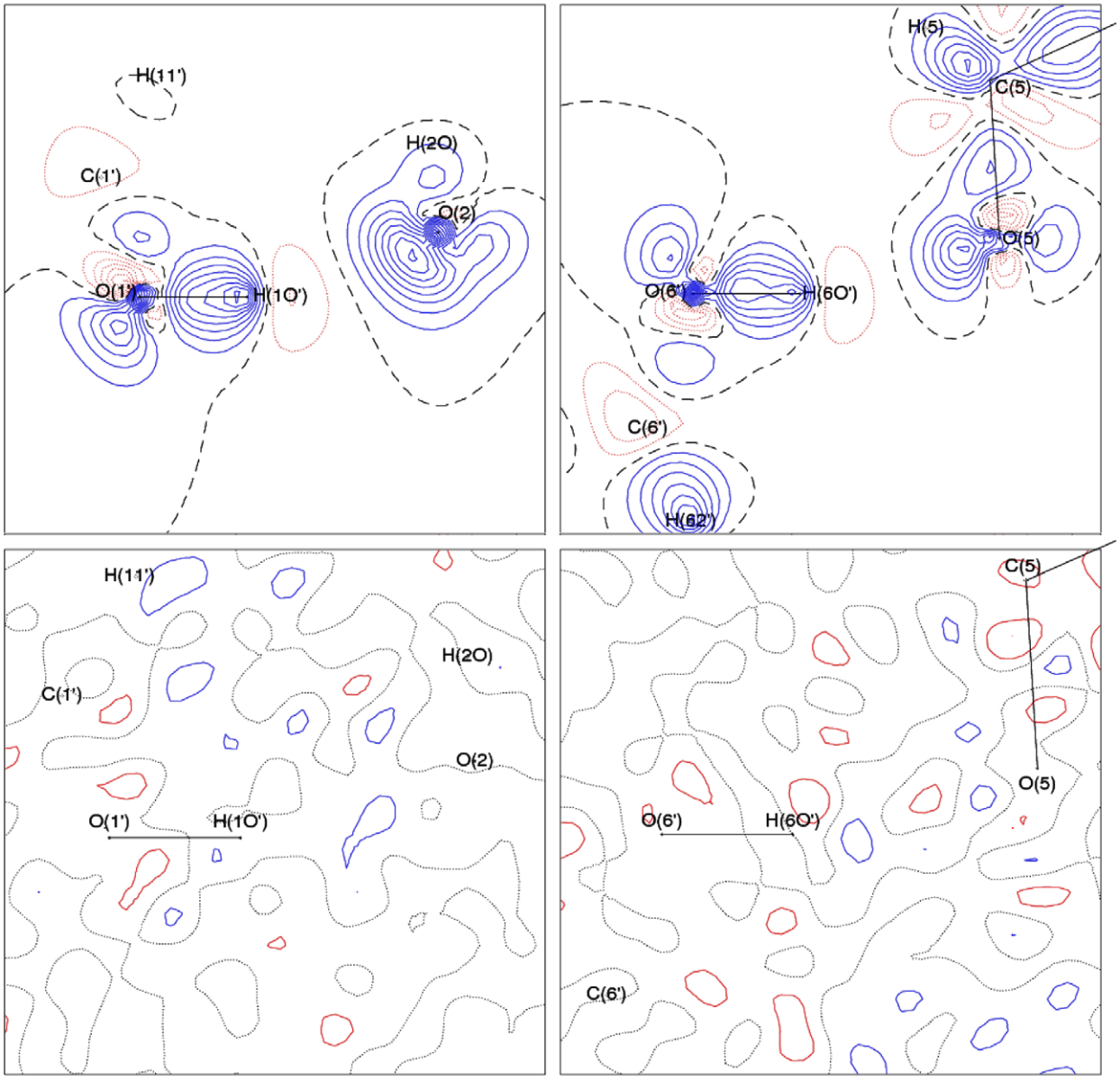

Figure 3. Static deformation density maps in the planes of the intramolecular HBs O(1′)H(1O′)···O(2) (top, left) and O(6′)–H(6O′)···O(5) (top, right), illustrating the charge rearrangement in one of the lone-pair lobes of the accepting O(2) and O(5)atoms. Positive, negative, and zero contours are represented by blue solid, red dotted, and black dashed lines, respectively. Contour intervals at 0.1 e Å^{-3}. Residual density maps in the planes of the intramolecular HBs O(1′)–H(1O′)···O(2) (bottom, left) and O(6′)–H(6O′)···O(5) (bottom, right), blue positive, red negative contours, contour intervals at 0.1 e Å^{-3}.

H(4O)···O(2′) and H(4O)···O(6) justifies these interactions to be considered as weak hydrogen bonds.

The acceptor–hydrogen distance (H···A) is in the range of 1.7438–2.4989 Å, while the angle (D–H···A) is found between 157.33° and 173.54° in all cases except for O(4)–H(4O)···O(2′) = 113.65°, which might be attributed to steric reasons.

The influence of hydrogen bonding on the experimental charge density was also studied quantitatively by means of topological properties as listed in Table 5. A relatively low value of the electron density and a positive Laplacian at the BCPs, observed in all cases, are indicative of closed-shell interactions.[24] The hydrogen-bond energies E_{HB} in Table 5, calculated with the relation 2, given by Espinosa et al.,[27] show that the nine HBs fall roughly into three groups, the stronger ones with E_{HB} >30 kJ mol^{-1}, the weaker ones with E_{HB} <30 kJ mol^{-1} and the very weak ones of the bifucated HB from the donating O(4) atom.

$$E_{HB} = 25{,}300 * \exp[-3.6 * (H \cdots A)] \text{ kJ mol}^{-1} \quad (2)$$

On the basis of experimental data for 83 hydrogen bonds occurring in 15 different compounds Espinosa et al. established fundamental correlations between geometrical, topological, and energetic parameters.[28,29] The data analyzed were drawn from experiments on different organic compounds performed in different laboratories under different experimental and refinement conditions. To explore the reproducibility of their results, we repeated their analysis by using the data of the nine hydrogen bonds in the crystal structure of sucrose considered in this study. Our data set is based on X-ray experiments, but the distances between hydrogens and the heavy atoms were set to the experimental neutron distances;[4] therefore, we made a comparison between our data of sucrose and those from only X-ray diffraction experiment and a combined experiment of both X-ray and neutron diffractions that are described in Ref. 28. The comparison was made by plotting the electron density, the Laplacian and the positive curvature λ_3 at BCPs of the HBs versus the O···H distances described in Table 5 and re-plotting the relations of Espinosa et al. (Fig. 4). In all cases, an exponential correlation is observed. For the electron density, the black solid line corresponding to a fit of parameters obtained in this work is in very good agreement with the green solid line corresponding to a fit of the combined experiment of both X-ray and neutron diffractions given by Espinosa et al. For the Laplacian the fit of this research is in good agreement with the fit of the X-ray experiment and is in a bad agreement with that of the combined experiment of X-ray and neutron diffractions. Espinosa et al.[28] reported 'Because $\nabla^2\rho(\vec{r})$ is the sum of the three principal curvatures, the dispersions found in the Laplacian plots are larger than those in the λ_3 plots and λ_3 is the best candidate for characterization and classification of HB

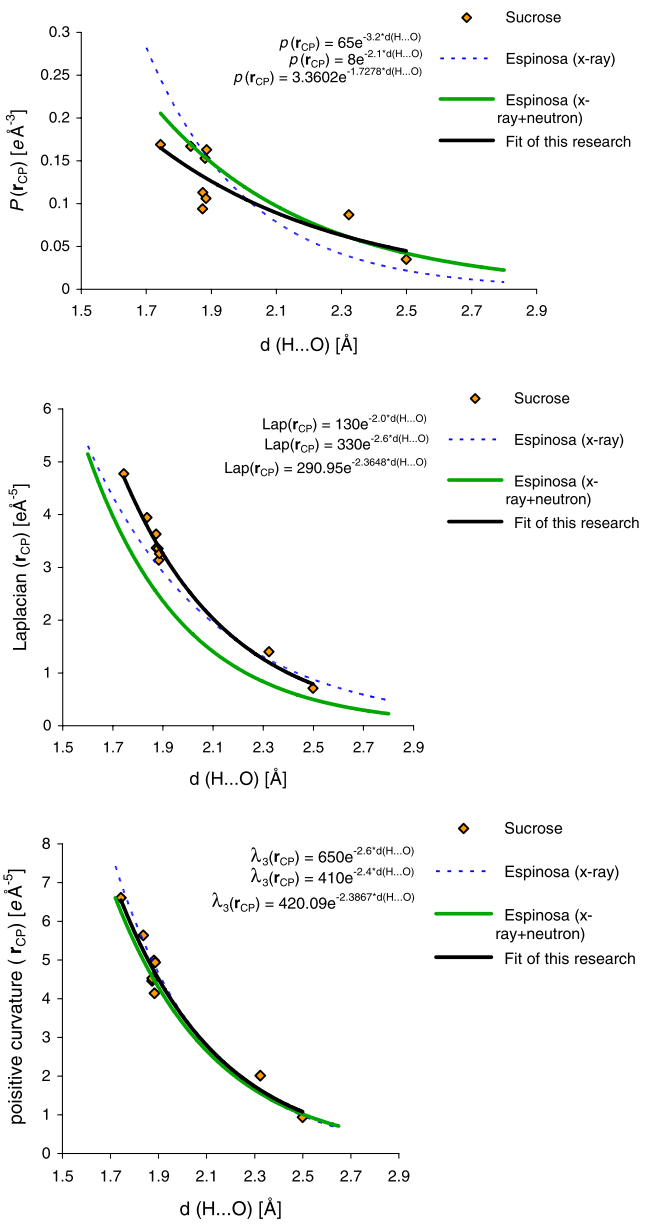

Figure 4. Hydrogen bond $\rho(\mathbf{r}_{CP})$ (top), $\nabla^2\rho(\mathbf{r}_{CP})$ (middle), and $\lambda_3(\mathbf{r}_{CP})$ (bottom) values of sucrose versus the d(H···O) distances. The Espinosa relations are also shown for comparison.

interactions'. In that respect a comparison of different Laplacian fits should be considered with care since it is less reliable than that of the positive curvature λ_3. The agreement in terms of the positive curvature λ_3 is especially excellent in all cases.

3.3. Electrostatic potential

For the consideration of the reactive behavior of a chemical system, the three-dimensional distribution of its electrostatic potential (EP) is very helpful in that negative regions can be regarded as nucleophilic centers, whereas regions with positive EP are potential

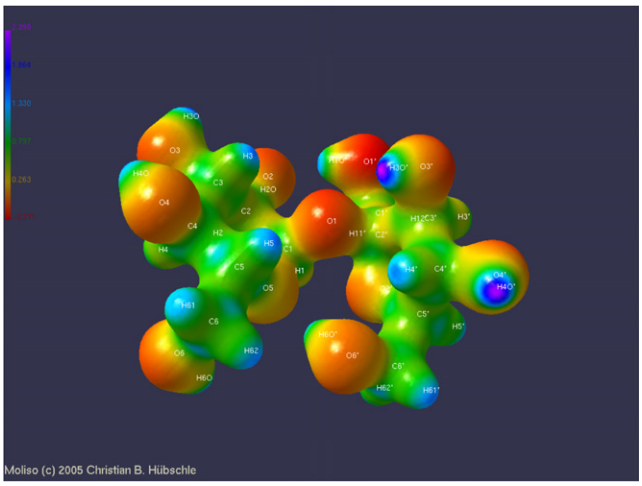

Figure 5. Experimental electrostatic potential, mapped by a color code (see color bar) on the electron-density isosurface at 0.5 e $Å^{-3}$ (Moliso representation).[35]

electrophilic sites. The EP, which can be derived directly from the electron density, was calculated from the experimental data using the method of Su and Coppens[30] and is represented in Figure 5 by a color code on the isoelectron-density surface at $\rho = 0.5$ e $Å^{-3}$. The EP makes the polarization of the electron density visible, in that, for example, noticeable negative electrostatic potential is seen around the oxygens, while pronounced positive EP regions are around the hydrogens. Moreover, it can be seen that the OH hydrogens, which are involved in hydrogen bonding, have a stronger positive EP than the hydrogens at the carbons being not involved in such interactions (see, e.g., the deep violet and hence strong positive region around H(40′), which is the donor H of the strongest hydrogen bond).

4. Conclusions

Based on a highly resolved X-ray data set ($\sin\theta/\lambda_{max} = 1.15$ $Å^{-1}$) of ~86,000 reflections measured at 20 K, a charge-density distribution of sucrose could be determined that allowed quantitative atomic, bonding and nonbonding topological properties to be derived making use of the procedures provided by Bader's AIM theory. Features like the increased strength of the endocyclic C–O bond to the anomeric carbon atom, variations of atomic volumes depending on their chemical environment and hydrogen-bond properties could be characterized. Since the time needed to collect X-ray data of several 10,000 reflections has been shortened drastically,[31,32] the experimental and methodical effort to study charge densities of medium-sized molecules of say 50–100 atoms is approaching a routine procedure, so that compounds like sucrose or larger carbohydrates can be the subject of charge-density analyses in time periods that are currently needed for the execution of a conventional X-ray analysis, provided that properly diffracting crystals of the compound in question can be grown. If modern database techniques are applied, as, for example, the invariom method developed in our group,[33,34] even low-resolution X-ray data sets are sufficient to yield reliable charge densities.

Acknowledgments

This work was financially supported by the Deutsche Forschungsgemeinschaft within the SPP1178 program and within the Graduate School 788 (Hydrogen Bonding and Hydrogen Transfer).

Supplementary data

Complete crystallographic data for the structural analysis have been deposited with the Cambridge Crystallographic Data Centre, CCDC No. 634580. Copies of this information may be obtained free of charge from the Director, Cambridge Crystallographic Data Centre, 12 Union Road, Cambridge, CB2 1EZ, UK (fax: +44-1223-336033, e-mail: deposit@ccdc.cam.ac.uk or via: www.ccdc.cam.ac.uk). Supplementary data also includes a table of energetic hydrogen bond quantities (Table S1) and a complete table of bond topological properties (with bonds to hydrogen atoms, Table S2). Supplementary data associated with this article can be found, in the online version, at doi:10.1016/j.carres.2007.04.004.

References

1. Bragg, W. L. *Proc. R. Soc. London, Ser. A* **1913**, *89*, 248–277.
2. Beevers, C. A.; McDonald, T. R. R.; Roberston, J. H.; Stern, F. *Acta Crystallogr.* **1952**, *5*, 689–690.
3. Brown, G. M.; Levy, H. A. *Science* **1963**, *141*, 921–923.
4. Brown, G. M.; Levy, H. A. *Acta Crystallogr., Sect. B* **1973**, *29*, 790–797.
5. Hanson, J. C.; Sieker, L. C.; Jensen, L. H. *Acta Crystallogr., Sect. B* **1973**, *29*, 797–808.
6. Longchambon, F.; Gillier-Pandraud, H.; Wiest, R.; Rees, B.; Mitschler, A.; Feld, R.; Lehmann, M.; Becker, P. *Acta Crystallogr., Sect. B* **1985**, *41*, 47–56.
7. Koritsanszky, T.; Strumpel, M. K.; Buschmann, J.; Luger, P.; Hansen, N. K.; Pichon-Pesme, V. *J. Am. Chem. Soc.* **1991**, *113*, 9148–9154.
8. Guillot, B.; Muzet, N.; Artecho, E.; Lecomte, C.; Jelsch, C. *J. Phys. Chem. B* **2003**, *107*, 9109–9121.
9. Koritsanszky, T. S.; Coppens, P. *Chem. Rev.* **2001**, *101*, 1583–1627.
10. Bader, R. F. *Atoms in Molecules: a Quantum Theory*, 1st ed.; Clarendon Press: Oxford, 1990.
11. Frisch, M. J.; Trucks, G. W.; Schlegel, H. B.; Scuseria, G. E.; Robb, M. A.; Cheeseman, J. R.; Zakrzewski, V. G.; Montgomery, J. A., Jr.; Stratmann, R. E.; Burant, J. C.;

Dapprich, S.; Millam, M. J.; Daniels, A. D.; Kudin, K. N.; Strain, M. C.; Farkas, O.; Tomasi, J.; Barone, V.; Cossi, M.; Cammi, R.; Mennucci, B.; Pomelli, C.; Adamo, C.; Clifford, S.; Ochterski, J.; Petersson, G. A.; Ayala, P. Y.; Cui, Q.; Morokuma, K.; Malick, D. K.; Rabuck, A. D.; Raghavachari, K.; Foresman, J. B.; Cioslowski, J.; Ortiz, J. V.; Baboul, A. G.; Stefanov, B. B.; Liu, G.; Liashenko, A.; Piskorz, P.; Komaromi, I.; Gomperts, R.; Martin, R. L.; Fox, D. J.; Keith, T.; Al- Laham, M. A.; Peng, C. Y.; Nanayakkara, A.; Gonzalez, C.; Challacombe, M.; Gill, P. M. W.; Johnson, B.; Chen, W.; Wong, M. W.; Andres, J. L.; Head-Gordon, M.; Replogle, E. S.; Pople, J. A. GAUSSIAN *98, rev. a.7*; GAUSSIAN: Wallingford, CT, 1998.

12. Popelier, P. L. A.; Bone, R. G. A. MORPHY *98, A Topological Analysis Program*; University of Manchester: Manchester, UK, 1998.
13. Messerschmidt, M.; Meyer, M.; Luger, P. *J. Appl. Crystallogr.* **2003**, *36*, 1452–1454.
14. SMART, SAINT; Bruker-AXS: Madison, WI, USA, 1996.
15. Sheldrick, G. M. SADABS & XPREP, *Programs for Data Reduction and Merging*; Göttingen University: Germany, 1997.
16. Sheldrick, G. M. SHELXS-*97, Program for Solution of Crystal Structures*; Göttingen University: Germany, 1997.
17. Sheldrick, G. M. SHELXL-*97, Program for Refinement of Crystal Structures*; Göttingen University: Germany, 1997.
18. Hansen, N. K.; Coppens, P. *Acta Crystallogr., Sect. A* **1978**, *34*, 909–921.
19. Koritsanszky, T.; Mallinson, R. P.; Howard, S. T.; Volkov, A.; Macchi, P.; Su, Z.; Gatti, C.; Richter, T.; Farrugia, L. J.; Hansen, N. K. XD—*A Computer Program Package for Multipole Refinement and Analysis of Charge Densities from Diffraction Data*; Freie Universität Berlin, 2003.
20. Clementi, E.; Roetti, C. *At. Data Nucl. Data Tables* **1974**, *14*, 177–478.
21. Burnett, M. N.; Johnson, C. K. ORTEP-III, Oak Ridge Thermal Ellipsoid Plotting Program for Crystal Structure Illustrations, ORNL-6895, Oak Ridge National Laboratory, 1996.
22. Volkov, A.; Abramov, Y.; Coppens, P.; Gatti, C. *Acta Crystallogr., Sect. A* **2000**, *56*, 332–339.
23. Volkov, A.; Gatti, C.; Abramov, Y.; Coppens, P. *Acta Crystallogr., Sect. A* **2000**, *56*, 252–258.
24. Koch, U.; Popelier, P. L. A. *J. Phys. Chem.* **1995**, *99*, 9747–9754.
25. Scheins, S. Ph.D. Thesis, Freie Universität Berlin, 2007.
26. Kalinowski, R. Diploma Thesis, Freie Universität Berlin, 2006.
27. Espinosa, E.; Molins, E.; Lecomte, C. *Chem. Phys. Lett.* **1998**, *258*, 170–173.
28. Espinosa, E.; Souhassou, M.; Lachekar, H.; Lecomte, C. *Acta Crystallogr., Sect. B* **1999**, *55*, 563–572.
29. Espinosa, E.; Lecomte, C.; Molins, E. *Chem. Phys. Lett.* **1999**, *300*, 745–748.
30. Su, Z.; Coppens, P. *Acta Crystallogr., Sect. A* **1992**, *48*, 188–197.
31. Luger, P.; Wagner, A.; Hübschle, Ch. B.; Troyanov, S. I. *J. Phys. Chem. A* **2005**, *109*, 10177–10179.
32. Förster, D.; Wagner, A.; Hübschle, Ch. B.; Paulmann, C.; Luger, P. *Z. Naturforsch., B: Chem. Sci.* **2007**, *B62*, 696–704.
33. Dittrich, B.; Koritsanszky, T.; Luger, P. *Angew. Chem., Int. Ed.* **2004**, *43*, 2718–2721.
34. Dittrich, B.; Hübschle, Ch. B.; Luger, P.; Spackman, M. A. *Acta Crystallogr., Sect. D* **2006**, *62*, 1325–1335.
35. Hübschle, C. B.; Luger, P. *J. Appl. Crystallogr.* **2006**, *39*, 901–904.
36. Abramov, Y. A. *Acta Crystallogr., Sect. A* **1997**, *53*, 264–272.